Dry Grinding: A More Sustainable Manufacturing Process for the Production of Automotive Gears

DRY GRINDING: A MORE SUSTAINABLE MANUFACTURING PROCESS FOR THE PRODUCTION OF AUTOMOTIVE GEARS

Alessandro Fortunato[a] Erica Liverani[a,d], Lorenzo Cestone[a], Flavia Lerra[c], Alessandro Ascari[a], Hambal Iqbal[a], Adrian H.A. Lutey[b]

(a) Dipartimento di Ingegneria Industriale (DIN), viale Risorgimento 2, Alma Mater Studiorum – Università di Bologna, Bologna, Italy

(b) Dipartimento Di Ingegneria E Architettura, Parco Area delle Scienze, 181/A, Università Degli Studi Di Parma, Parma, Italy

(c) Ferrari S.p.a, Viale Enzo Ferrari 27 I-41053 Maranello, Modena, Italy

(d) **Corresponding author: erica.liverani2@unibo.it., https://orcid.org/0000-0002-0010-6871, viale Risorgimento 2, 40136 Bologna, BO, Italy**

Abstract

Gears represent a fundamental component of automotive transmissions, the performance of which is directly influenced by flank surface integrity. With the exception of grinding, gear production does not require the use of lubricants. The elimination of oils in the final finishing phase represents an important opportunity to greatly improve process sustainability and reduce production costs. However, dry grinding presents several challenges, including dimensional tolerances and roughness requirements, microstructural defects due to excessive heat generation, and maintaining the overall surface integrity of flanks such that wear resistance is not compromised. The present work investigates the geometric accuracy, microstructure and wear resistance of FIAT 500 4/6 speed gears manufactured by FCA/Stellantis, comparing conventional wet grinding with two alternative processes including superfinishing and dry grinding. The material and manufacturing processes employed prior to grinding were the same in all cases, with grinding then performed by the same manufacturer. The dimensional accuracy, roughness, microstructure, residual stress state and wear resistance of gear flanks were then analysed to compare the overall performance of each grinding process. The obtained results show that dry grinding can produce gears with acceptable geometric accuracy, no microstructure defects and greater wear resistance than gears finished with conventional wet grinding or superfinishing. As a result, the complete elimination of lubricant in gear production is possible, leading to a more sustainable process without compromising gear performance.

Keywords: Dry grinding; Gears; Sustainable technology; Surface Integrity

1. INTRODUCTION

Electrification of automotive powertrains over the coming years will see an increase in gear production, particularly for battery-electric vehicles. Making the gear production chain more sustainable is thus essential. Wire electric discharge machining (WEDM) and gear rolling represent potential one-step processes for the production of gears [1]; however, mass production of high-performance gears such as those employed in automotive powertrains currently requires the following stages: turning, named also “soft turning” because the process involved non-hardened steel, soft hobbing of teeth, de-burring, heat treatment and finishing of the hardened surface [2]. Gear finishing aims to eliminate geometric errors remaining after hobbing and heat treatment. This phase represents a necessary final step to achieve two important goals: maximize load capacity and minimize running noise [3]. Although many cutting and grinding processes can generate sufficient surface integrity and a compressive residual stress state within the surface and subsurface regions, continuous generating grinding is most suitable as it reduces thermal damage [4]. Compared to conventional grinding methods, continuous generating grinding maintains lower temperatures, minimizing thermal and metallurgical alterations. This results in better preservation of the material's mechanical properties. Car manufacturers therefore most commonly perform grinding with a worm grinding wheel, which also has the advantage of being very fast. On the other hand, the conventional grinding processes produce large amounts of thermal energy, leading to heat generation and temperature rise [5]. This in turn leads to accelerated wear of abrasive grit within grinding wheels and thermal damage of the machined surface. Alteration of the finished surface can compromise the functional performance of components utilized in a variety of industrial sectors, including gears [3]. In order to avoid this problem, a large amount of lubricant is currently used, with energy consumption for lubrification and cooling representing more than 60% of the total energy consumption of a typical grinding machining centre [6]. Focus must therefore be placed on reducing the amount of grinding fluid used while maintaining surface quality, thus reducing associated energy and environmental problems.

To accomplish this, a variety of steps can be taken. For instance, reducing waste and using less mineral-based cutting fluids leads to a more environmentally friendly method of manufacturing gears. In order to satisfy global goals in terms of carbon neutrality, researchers have thus focused more on finding ways to reduce thermal damage during dry grinding processes [7]. Several papers have focused on evaluating the effects of grinding tools and process parameters in relation to dry grinding, with promising results [8,9, 10]. Others have been sought to better understand heat generation during surface grinding to identify ways of minimizing heat damage. Kizaki et al. [11] provided insight into

temperature evolution and heat generation during continuous generating grinding, demonstrating that a specific grinding energy reduction is possible by increasing the pitch or number of teeth of the gears. Jamshidi H. and Budak E. [12] reached the same conclusions using a backward approach that excluded from the parameters those that caused surface defects such as burns and oxide layer formation. High surface temperatures and/or exposure time effectively result in a rehardened zone known as the "white layer," which extends from the ground part's surface inside the component to its interior. Below this is a "dark tempered layer," which has a low hardness. Microstructural defects such as burns, or white layer development primarily influence the wear resistance of a gear. Hard finishing of gears must also achieve high load capacity and low operating noise. Thus, it is crucial to strictly adhere to the defined flank geometry and reduce form errors [13]. Finally, the overall integrity of gear surfaces must also be assessed in terms of roughness, surface topography and residual stresses, which have a significant impact on component performance in terms of fatigue life [14], contact conditions, wear, tribology, and lubrication [15], with these factors often inter-related. Several investigations based on numerical simulation and experiments have been carried out to better understand correlations between gear fatigue life and surface integrity. Zhang et al. [16] investigated the impact of surface roughness on gear contact fatigue life using numerical simulations, finding that fatigue life is most strongly influenced by surface roughness rather than conditions within the subsurface region, suggesting that micropitting failure is more likely to occur as roughness increases. Wang et al. [17] found that pitting and deep spalling failures are less likely as surface hardness and hardness depth increase. By numerically assessing the effects of residual stress induced by surface treatments on gear contact fatigue, Liu et al. [18] found that compressive residual stress may reduce the resultant stress. They analysed the time-varying multi-axial stress states during contact, the Matake, Findley, and Dang Van multi-axial fatigue criteria were utilized to calculate the critical planes and resultant stress. The mutual impact of different surface integrity factors on contact fatigue has also been investigated by some authors. Cui et al. [19] found that the damage evolution rate firstly decreases then increases as surface residual compressive stress and hardness rise. The rate at which damage evolves increases with higher surface roughness. Using a fatigue probability model, Hultgren et al. [20] observed that fatigue performance increases non-linearly with decreasing surface roughness and increasing amplitude of compressive residual stress. Zhang et al. [21] evaluated the correlation between different surface integrity parameters and gear fatigue performance. The three main parameters affecting gear contact fatigue were found to be surface hardness (37%), maximum compressive residual stress (40%) and surface roughness (23%). In relation to wear phenomena, several papers state that macro-pitting is associated with asperity deformation and accompanying microstructural changes, deformation bands and plastically deformed regions [22,23]; however, a unified mechanism relating to micro-

pitting has not yet been established due to the presence of different influencing factors. In light of the aforementioned considerations, this paper aims to examine three distinct grinding techniques and assess outcomes in terms of gear performance and surface integrity. Three grinding processes were selected based on current manufacturing standards and new requirements for carbon neutrality: i) wet grinding, the most commonly employed finishing process, serving as a benchmark; ii) dry grinding, performed without the use of lubricants; and iii) superfinishing, a wet process that has been shown to increase micro-pitting life [24]. Among the abovementioned processes, wet grinding is widely used by gear manufacturers [25]. To provide a useful comparison for car manufacturers, FIAT 500 4/6 speed gears, made from 27MnCr5 and manufactured by FCA/Stellanti, were employed for all experiments. All gears were produced by FCA at the Verrone plant (Italy) and subject to the same process chain prior to grinding, including turning with a reduced amount of lubricant (named "green turning"), hobbing, chamfering and heat treatment. After grinding, all gears were analysed with an optical microscope and SEM for microstructure evaluation, an optical profiler for acquisition of the surface topography and roughness, a Klingelnberg measuring system for evaluation of geometric errors and an XRD microscope for residual stress measurement. Finally, wear tests were performed to evaluate the influence of grinding on gear durability.

2. MATERIAL AND METHODS

2.1 Gear properties and requirements

A standard helical automotive gear, commonly employed for the 4/6-speed of six-speed gearboxes in modern motor vehicles, was selected for the study. The gears were made from 27MnCr5 (1.7147) carburized case-hardened steel with chemical and mechanical properties in line with EN10084:2008, representing one of the most common choices for automotive transmission components. Before finishing, all gears were subjected to green turning and hobbing, followed by heat treatment to improvement surface hardness. In order to achieve an effective case depth of 0.35 0.65 mm with a surface hardness of 59-65 HRC after grinding, the heat treatment involved vacuum carburizing and gas quenching followed by stress relieving. Microstructure and microhardness analysis of one gear before the subsequent grinding process was carried out and reported in Figure 1. The mean subsurface hardness value (from 35 to 100 μm from the surface, as explained in Section 2.3.3) was calculated by repeating the analysis 5 times, and the final value of 1070±65 HV0.2 was obtained.

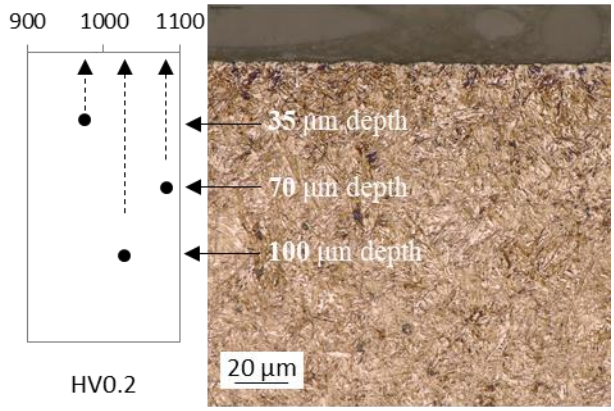

Figure 1 Microstructure and microhardness analysis before the grinding process

The final machining phase comprised grinding of the transmission gears, the topic of the present investigation. Grinding is the most precise production step and determines the final quality of the gear in terms of geometric accuracy and surface integrity. With a crucial part to play in transmission efficiency and noise, flank geometry and surface roughness have a significant impact on transmission performance. While the grinding process is typically optimized to meet geometric requirements and achieve low roughness, current specifications also place a strong emphasis on gear endurance. In particular, thermal damage to the surface must be prevented and a compressive residual stress state must be ensured in order to increase the wear resistance of gears. Details relating to specific requirements from the car manufacturer are reported in Table 1.

Table 1: Final gear quality requirements

Maximum roughness Ra	0.6 µm
Maximum profile form error ffα	6 µm
Maximum helix form error ffβ	5.5 µm
Helix crowning range cβ	4 ± 2 µm
Burn and white layer	Absent

Three different grinding processes were examined, starting with the reference procedure currently employed for grinding of automotive gears. The grinding cycle parameters and grinding wheel specifications were changed depending on the grinding process employed, including optimized wet grinding (WG), dry hard finishing (DHG) and superfinishing (SG). The initial phase of the work focused on optimizing process parameters, with results compared in terms of dimensional accuracy, roughness and microstructure to identify the best combination of parameters for achieving the best level of surface integrity and satisfy the aforementioned requirements.

2.2 Grinding processes and experimental setup

Experiments were performed by comparing three different grinding processes: i) conventional wet grinding, ii) dry hard grinding and iii) superfinishing. For wet and dry grinding, three different conventional grinding wheels (GW-1, GW-2 and GW-3) were adopted, with specifications as reported in Table 2. The wheel diameter and width were kept constant, equal to 250 mm and 100 mm, respectively. Superfinishing instead employed a dual grinding wheel made up of two different parts with different grain sizes, where larger grains were adopted for roughing and smaller grains for finishing. The part used for roughing had 120-grit abrasive grains while the part used for finishing had 180-grit abrasive grains. Specifications relating to the grinding wheels employed for the superfinishing process (D-GW-1 and D-GW-2) are reported in the final two columns of Table 2. The underlying parameters come after preliminary trials. For each category, the best compromise was found based on microstructural results.

Table 2: Grinding wheel (GW) specifications

Parameters	GW-1	GW-2	GW-3	D-GW-1	D-GW-2
Abrasive grain material	Silicon carbide	Fused aluminium oxide	Fused aluminium oxide	Fused aluminium oxide	Silicon carbide
Grit size	120	120	120	120/180	120/180
Binder type	Vitrified	Vitrified	Vitrified	Vitrified	Vitrified
Binder hardness	J	N	II	II	J
Structure	18	13	11	9/8	18

2.2.1 Wet grinding

Considering that wet grinding is a commonly adopted process for finishing transmission gears, constant process parameters corresponding to established state-of-the-art procedures were employed, as reported in Table 3.

Table 3. Wet grinding process parameters

Grinding phase	Cutting speed [m/s]	Stock [μm]	Feed rate [mm/rev]	Shift/mm sh [mm]	Back shift [mm]
(1) Normalizing		30	1.1	0.04	0
(2) Roughing	80	50	0.9	0.04	0
(3) Finishing		20	0.4	0.03	7.3

Different grinding tools were nonetheless employed to identify potential improvements in durability and effectiveness compared to current solutions. Thus, three test conditions were evaluated using the process parameters reported Table 3 and grinding wheels given Table 2. Wet grinding performed with the GW-1 grinding wheel was referred to as WET-1, while the same process carried out with GW-2 and GW-3 grinding wheels was referred to as WET-2 and WET-3, respectively. A G160 grinding machine (Samputensili Machine Tool Srl) was used for wet grinding, with the main technical data reported in the first column of Table 4. Constant oil temperature of 24 °C, oil pump pressure of 15 bar and oil flux of 88 L/min were maintained during all tests.

Table 4. Grinding machine specifications

	G160	SG160 SKYGRIND	G250
Workpiece diameter max [mm]	160	160	250
Module range [m_n]	1-3	1-3	0.5-7
Face width max [mm]	300	300	550
Helix angle degree	+95°/-45°	+45°/-45°	+45°/-45°
Grinding wheel diameter [mm]	210-275	210-250	170-250
Grinding wheel width [mm]	100	100	180
Grinding speed max [m/s]	80	80	80
Dressing tool diameter [mm]	132	132	120
Siemens control system		Sinumerik 840 D sl	

2.2.2 Dry hard grinding

Dry hard grinding consisted of two phases, skiving and grinding, with the overall stock removal being 100 μm in all cases. Experiments were performed in two steps. The first considered six different configurations, defined using the grinding wheels in Table 2 and two different values of feed rate.

The second began by choosing the best grinding configuration in terms of surface integrity from the previous step and employing a double grinding pass strategy. Skiving was carried out to remove 90 µm of the stock with a hob in all cases, while grinding was performed to remove the remaining 10 µm using both a single and double-pass strategies, with two consecutive passes at
5 µm in the latter case. Skiving removed material in an up-grinding mode, while grinding was performed in a down-grinding mode to reduce heat generation during the process. Details of each grinding configuration are reported in Table 5.

Dry grinding performed with the GW-1 grinding wheel was referred to as DRYs-1(a,b), while the same process carried out with GW-2 and GW-3 grinding wheels was referred to as DRYs-2(a,b) and DRYs-3(a,b), respectively. Set up (a) adopted a feed rate of 0.34 mm/rev, while set up (b) adopted a feed rate of 0.54 mm/rev. Finally, DRYd was carried out with the GW-3 grinding wheel, a feed rate of 0.34 mm/rev and two passes with 5 µm stock each.

A Samputensili SG160 SKYGRIND grinding machine was used for dry grinding, with the main technical data reported in the second column of Table 4. The grinding machine, characterized by two spindles, was designed for mass production of automotive gears.

Table 5. Dry hard grinding process parameters

Skiving	*Cutting speed [m/s]*	*Feed rate [mm/rev]*	*Shift/mm sh [mm]*	*Stock p [µm]*
	2.5	2.27	-	90
Grinding Setup	DRYs-1(a,b)	DRYs-2(a,b)	DRYs-3(a,b)	DRYd
Grinding Wheel	GW-1	GW-2	GW-3	GW-3
Cutting speed [m/s]		80		
Stock p [µm]	10	10	10	5 + 5
Feed rate [mm/rev]	0.34(a), 0.54(b)	0.34(a), 0.54(b)	0.34(a), 0.54(b)	0.34
Shift/mm sh [mm]		1.026		

2.2.3 Superfinishing

Superfinishing process parameters are summarized in Table 6. The roughing phase consisted of two passes with a constant stock of 45 µm and 40 µm, respectively, while the finishing phase consisted of two passes with a variable depth of cut: 12.5 + 2.5 µm for a low-load setup defined as L and 10 + 5 µm for a high-load setup defined as H. Four configurations were therefore tested with the grinding wheels defined in Table 2. Superfinishing processes performed with the D-GW-1 grinding wheel were

referred to as SF-L1 and SF-H1, while the same processes performed with the D-GW-2 grinding wheel were referred to as SF-L2 and SF-H2.

A Samputensili G250 grinding machine was used for superfinishing experiments, with the main technical data reported in the third column of Table 4.

Table 6. Superfinishing process parameters

	Pass	*Cutting speed [m/s]*	*Stock p [µm]*	*Feed rate [mm/rev]*	*Shift/mm sh [mm]*
Roughing	*1*	*60*	*45*	*0.55*	*0.855*
	2	*60*	*40*	*0.5*	*0.855*
Finishing SF-L	*1*	*60*	*12.5*	*0.2*	*0.513*
	2	*60*	*2.5*	*0.2*	*0.513*
SF-H	*1*	*60*	*10*	*0.2*	*0.513*
	1	*60*	*5*	*0.2*	*0.513*

2.3 Surface integrity analysis

Evaluation of experimental outcomes to determine the grinding setup achieving best Surface Integrity (SI) was based on assigning a hierarchic weight to the final results. The following SI parameters and criteria were considered, in order of significance:

- Roughness: the final Ra value must not exceed the reference value of 0.6 µm.
- Geometric accuracy: waviness parameters and requirements must comply with those specified in Section 2.3.1.
- Microstructure: gear flank surfaces must be free from grinding burn damage, classified according to three levels depending on the amount of heat generated: i) oxidation (dark layer formation), ii) white layer formation and iii) cracking due to thermal deformation [26]. These defects result in localized changes in hardness (softening and re-hardening) of gear flanks, which may ultimately cause transmission wear, vibration and noise.
- Hardness: in addition to the strict requirements of the gears, the subsurface hardness after grinding was evaluated to highlight and compare the thermal effects of different machining processes.

The methodology employed for the detailed evaluation of SI is provided in the following sections.

2.3.1 Dimensional analysis

The dimensional accuracy of gears was evaluated by comparing the design geometry with the actual geometry upon completion of all machining operations. Dimensional analysis can be carried out considering both the macro- and micro-geometric accuracy. Macro geometry can be described in terms of deviations in tooth spacing and profile and helix slope due to process kinematics (machine structure and motion of controlled axes) and wheel dressing operations. Micro geometry can be described in terms of tooth surface roughness and waviness due to the machining process and parameters. For the purpose of this work, macro-geometric accuracy was not considered due to the use of industrial machines and procedures for wheel dressing. On the other hand, micro-geometric accuracy was assessed due its dependence on the machining process and parameters. The roughness of the ground gear flanks was therefore assessed, together with profile and helix shape deviations. Gears were mounted on a shaft, with tooth contours obtained using a Klingelnberg measuring system employing a touch probe for measurements in the profile and lead directions.

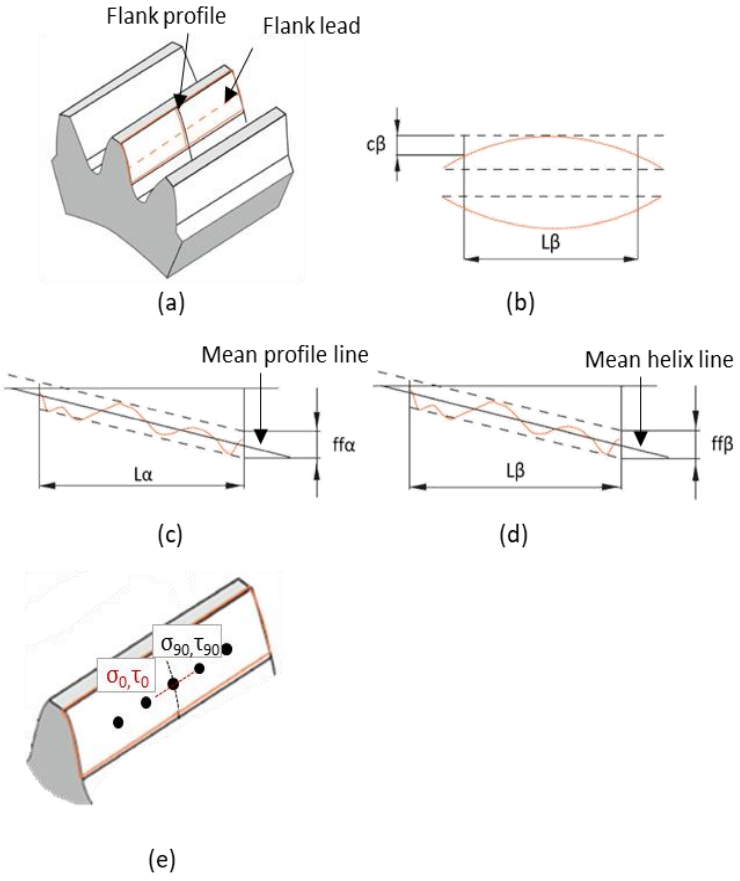

Figure 2 Representation of flank profile and helix (a), helix crowning cβ (b), profile deviation ffα (c), helix deviation ffβ (d) and probes for residual stress measurements (e)

The dimensional characteristics that were assessed, shown schematically in Figure 2, were as follows:

1. cβ is helix crowning, representing the chordal thickness of the tooth along its axis within the lead inspection range Lβ (Figure 2b).
2. ffα is the profile form deviation, measured as the distance between two lines parallel to the mean profile line that contains the real profile, in the evaluation range Lα (Figure 2c).
3. ffβ is the helix form deviation, measured as the distance between two helical lines parallel to the mean helix that contains the real profile, in the evaluation range Lβ (Figure 2d).

2.3.2 Surface analysis

Profile and lead roughness measurements were performed on three teeth of each gear using a Klingelnberg P65 measuring system. Average roughness values were determined based on measurements performed on both left and right flanks. Linear roughness parameters Ra and Rt were determined for each grinding configuration to allow direct comparison with process quality requirements. Coherence scanning interferometry (CSI) was then performed for detailed acquisition of the surface topography of gear tooth flanks after each grinding process with a Taylor Hobson TalySurface CCI optical profiler with 10× objective. Areal roughness parameters Sa, Ssk and Sku were determined in line with ISO 25178 based on five measurements performed at the center of the flank, near the tip and root of the flank profile and near the start and end of the flank lead of each gear. A quadratic form filter was applied to remove the flank curvature prior to calculation of all areal roughness parameters.

2.3.3 Microstructural evaluation and hardness measurements

Microstructural evaluation was performed by polishing and chemically etching gear tooth cross sections cut from gears finished with each grinding process. Sample preparation and etching were undertaken in line with DIN EN ISO 14,104:2014 (E) (ISO/DIS 14104) and DIN ISO EN 643 (ISO 643). This method made it possible to observe grinding burns that had developed as a result of high thermal loads produced during finishing. Metallurgical specimens were etched with Nital3% reagent (3% nitric acid in a carrier solvent of ethyl alcohol) for 5 s. Defects were analyzed by measuring their extension into the tooth depth using an optical microscope (OM, Zeiss Axio Vert.A1M) with a magnification of 20×. Both right and left flanks were analysed in all cases.

Following the microstructural assessment, a hardness profile was performed from 35 μm to 1 mm in-depth, perpendicular to the flank surface before grinding (Section 2.1) and after each optimized

grinding process. Using a ZwickRoell Vickers microhardness tester, a 200 g load was applied for 15 seconds, and at least three repetitions were carried out for each depth.

2.3.4 Residual stress measurements

The measurement of residual stress completed the Surface Integrity characterization. Since there are no particular requirements regarding residual stress, these data were not used as a criterion for selecting grinding processes. Residual stress measurements were performed with an AST X-Stress 3000 portable X-ray diffractometer equipped with CrKα radiation. Normal and shear stresses in the flank profile (σ_0, τ_0) and lead (σ_{90}, τ_{90}) directions were performed on the as-ground flank of one tooth for each selected gear. Five measures were performed along a line in the middle of the flank, between the top and root of the tooth, with a distance between each point of 2 mm as shown schematically in Figure 2e.

2.4 Gear wear tests

The main objective of the study was to evaluate wear resistance after different grinding processes and identify correlations between wear resistance and SI. Process parameter sets providing the best compliance with the SI parameters were identified for each process. Wear tests were carried out using a modified FZG test device, shown in Figure 3, specifically designed for the study following guidelines within BS ISO 14635-2:2004. Loading of the test gears could be adjusted by applying appropriate torque to shaft 1 through the loading mechanism indicated by the number 2 in Figure 3. All tests were carried out with the same torque, 350 Nm, defined based on preliminary tests. Specifically, the test torque load was defined as the minimum value that led to wear initiation after 1.5 million cycles under all of the selected grinding conditions. The applied torque was measured on-line with a torque sensor, which was also equipped with an encoder for counting shaft revolutions. Tests were performed with lubricating oil (synthetic gear oil ISO VG 320) with an inlet temperature of 45 °C and flow rate of 2.0 L/min. Tests were terminated after 1.5 million cycles. The flanks of all gear teeth were examined for wear identification at the end of tests. Images of each tooth flank were obtained by mounting the gear on a dividing head positioned below a stereo microscope (ZEISS Axiocam 105 color), as shown in Figure 3b. ImageJ software was then used to calculate the extension of the damaged surface on each tooth, with the following equations used for comparison of wear in each case.

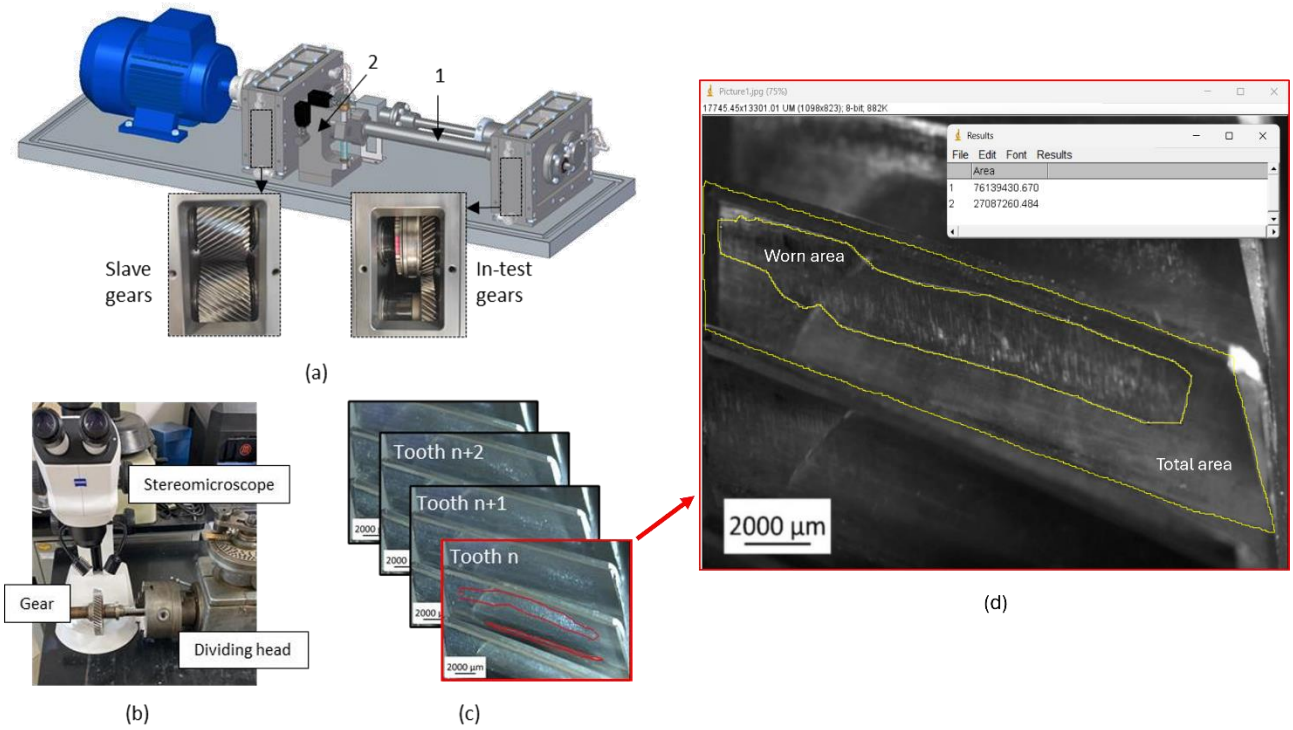

Figure 3(a) Main elements of the gear testing machine, (b) microscopic image acquisition setup (c) Measured teeth on the gear and (d) example of data acquisition from ImageJ software for total area and damaged area measurements

Equation 1 $$A_{w,t}[\%] = 100\frac{A_{w,ti}\,[mm]}{A_f\,[mm]}$$

Equation 2 $$A_{w,gi}[\%] = \frac{\sum_1^n A_{w,ti}}{n \cdot A_f}$$

Equation 3 $$A_{w,p}\,[\%] = \frac{\sum_1^m A_{w,gi}}{m}$$

where $A_{w,\,t}$ represents the damage percentage on one tooth flank, defined as the ratio of the worn area, measured by Image J ($A_{w,\,ti}$) (area identified in Figure 3c) and flank area (A_f), $A_{w,gi}$ is the mean worn area of the ith gear, calculated as the mean damage of all flanks on one gear, and $A_{w,p}$ is the average wear area of the group of gears manufactured with the same grinding process.

A SEM-FEG microscope (Tescan Mira3 with Schottky emitter) was then utilized to conduct wear analysis after evaluating the damaged area. The flanks of three teeth from one gear obtained with each grinding setup were analyzed.

3. RESULTS

3.1 Wet grinding optimization

Klingelnberg measurements of dimensional tolerances for gears finished with wet grinding are shown in Figure 4 in terms of helix crowning cβ, profile deviation ffα and helix deviation ffβ. All wet grinding tests were in line with the initial requirements stated in Table 1. Contours acquired for both the profile and lead were very smooth.

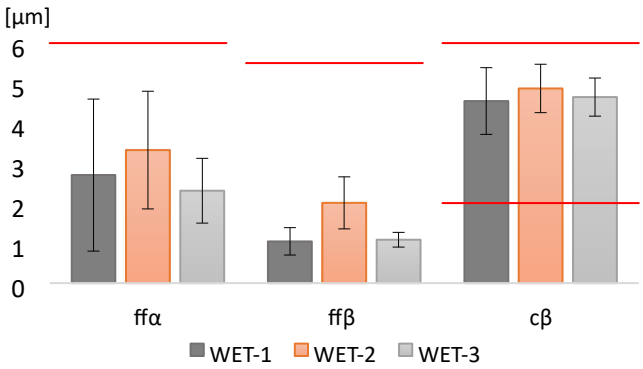

Figure 4 Dimensional tolerance measurements for wet grinding

Roughness parameters Ra and Rz are reported in Table 7 for both the tooth profile and lead. Wet grinding led to comparable Ra roughness values of approximately 0.2 µm for all tested setups.

Table 7. Measured roughness parameters for wet ground gears

	Profile Ra [µm]	*Std. Dev*	*Profile Rz [µm]*	*Std. Dev*	*Lead Ra [µm]*	*Std. Dev*	*Lead Rz [µm]*	*Std. Dev*
WET-1	*0.22*	*0.012*	*1.30*	*0.096*	*0.12*	*0.03*	*0.65*	*0.11*
WET-2	*0.20*	*0.009*	*1.33*	*0.072*	*0.10*	*0.02*	*0.66*	*0.07*
WET-3	0.19	0.013	1.27	0.090	0.11	0.01	0.72	0.06

The microstructures of samples obtained with the wet grinding process are reported in Figure 5. For each setup, the microstructure along the left and right flanks was acquired towards the flank and in correspondence with the tooth tip, with one representative picture presented for each sample. The microstructure did not contain obvious defects with the first setup, WET-1 (Figure 5a), while the second (WET-2) and third (WET-3) setups instead presented a darkened layer, shown in Figure 5b and 5c, respectively. WET-3, employing a conventional fused aluminum oxide abrasive (GW-3 in

Table 2), showed a deeper darkened layer (around 30 µm) compared to that obtained with WET-2 (around 20 µm), which employed a mix of pink and white aluminum oxide abrasive.

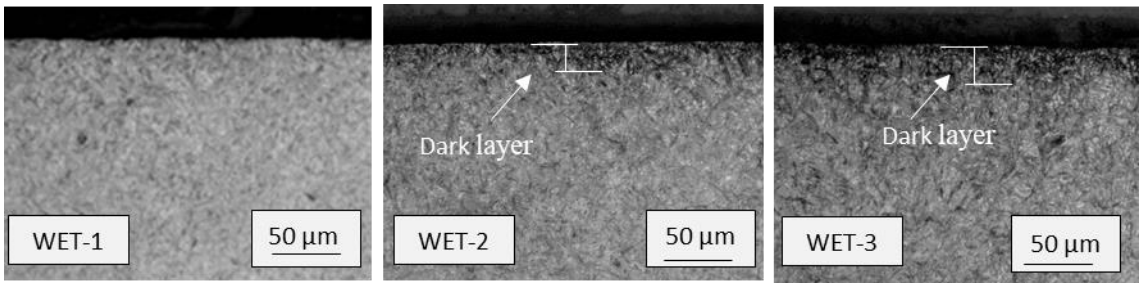

Figure 5 Microstructural analysis of samples obtained with wet grinding using process setups WET-1 (a), WET-2 (b) and WET-3 (c)

Comparing the obtained data in terms of dimensional accuracy, surface roughness and microstructure in Table 8, WET-1 was considered the optimal set-up for the wet grinding process.

Table 8. Summary of results obtained with wet grinding.

	Profile Ra [µm]	*Lead Ra [µm]*	*Ffα [µm]*	*Ffα [µm]*	*cβ [µm]*	*Dark layer*	*White layer*
Reference	< 0.6	< 0.6	< 6	< 5.5	4 ± 2	no	no
WET-1	✓	✓	✓	✓	✓	✓	✓
WET-2	✓	✓	✓	✓	✓	×	×
WET-3	✓	✓	✓	✓	✓	×	×

3.2 Dry hard grinding optimization

Klingelnberg measurements of dimensional tolerances for all gears finished with dry hard grinding are shown in Figure 6, while roughness values are reported in Table 9.

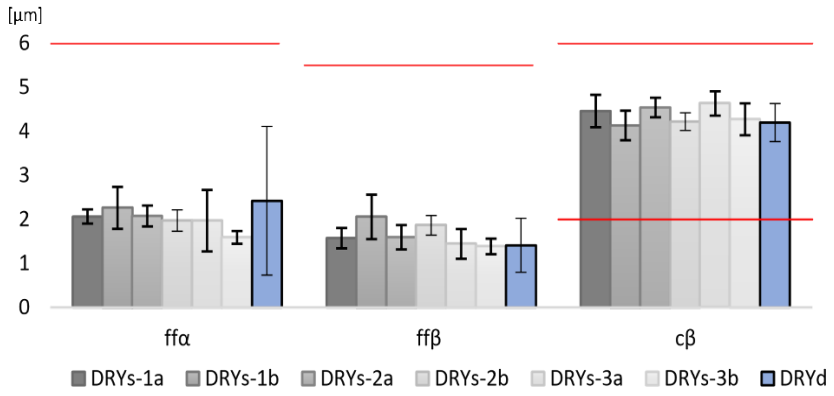

Figure 6 Dimensional tolerance measurements for dry grinding

Table 9: Measured roughness parameters for dry ground gears

	Profile Ra [µm]	*Std. Dev*	*Profile Rz [µm]*	*Std. Dev*	*Lead Ra [µm]*	*Std. Dev*	*Lead Rz [µm]*	*Std. Dev*
DRYs-1a	0.31	0.027	2.12	0.298	0.18	0.066	1.16	0.422
DRYs-1b	0.38	0.029	2.46	0.390	0.23	0.059	1.56	0.355
DRYs-2a	0.24	0.015	1.60	0.200	0.10	0.009	0.69	0.061
DRYs-2b	0.28	0.011	1.93	0.194	0.15	0.033	0.95	0.184
DRYs-3a	0.40	0.018	2.49	0.110	0.23	0.047	1.53	0.274
DRYs-3b	0.42	0.009	2.63	0.208	0.22	0.052	1.51	0.361

The GW-2 grinding wheel (set up DRYs-2(a,b)) produced the lowest roughness, with an average value of Ra < 0.3 µm. Despite the coarser grain size of the selected wheel, the lower roughness was achieved as a result of the harder binder. This can be attributed to the grains' fast wear and flattening when a grinding wheel with coarse grains and a hard binder is used. As a result of the smoother wheel surface, the maximum allowable allowance is reduced, but the roughness of the gear tooth is improved. Nevertheless, in that condition the contact area increases and produces more heat during the grinding process, leading to higher temperatures and an increased risk of surface burning.

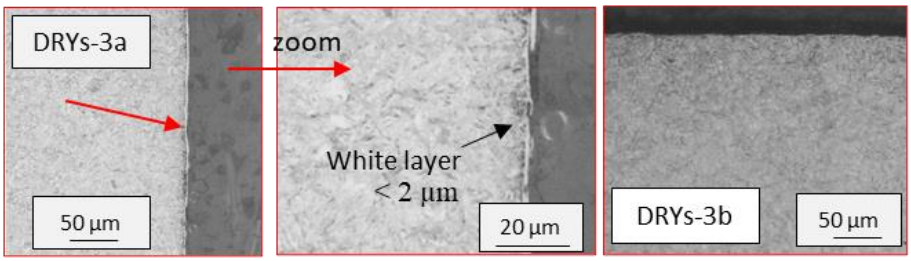

Figure 7 Microstructural analysis of samples obtained with dry hard grinding using process setups DRYs-3a (a) and DRYs-3b (b)

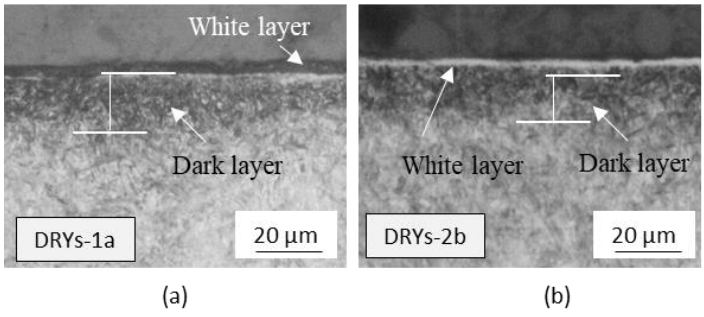

Figure 8 Microstructural analysis of samples obtained with dry hard grinding using process setups DRYs-1a (a) and DRYs-2b (b)

The microstructures of samples obtained with dry grinding were acquired in the same positions as for wet grinding. Figures 7 and 8 show the microstructure obtained with setups DRYs-3 and DRYs1. In the form case, the microstructure did not contain obvious defects except for a thin white layer less than 2 µm in thickness towards the right flank lead, visible in the high-magnification image in Figure 7a (DRYs-3a). The setup adopting the GW-1 grinding wheel (c) and a feed rate of 0.34 mm/rev (DRYs-1a) produced a microstructural with a thin white layer less than 2 µm in thickness close to the tip, together with a slightly darkened layer (Figure 8a). White and darkened layers were also visible towards the left flank lead. The DRYs-2b setup (0.54 mm/rev) exhibited more substantial thermal defects along both flanks (Figure 8b). A white layer up to 5 µm in thickness and a darkened layer of up to 20 µm were detected. Similarly, but with a wider extension, the DRYs-2 setup led to substantial thermal burns characterized by an average white layer thickness of around 4 µm (DRYs-2a), up to a maximum of 8 µm in correspondence with the right flank tip using a feed rate of 0.54 mm/rev (DRYs-2b), and a maximum darkened layer of around 20 µm at both feed rates. Given that all dry hard grinding configurations led to dimensional and roughness tolerances being respected, Table 10 provides a summary of microstructural analyses comparing the results of dry hard grinding obtained with the different process setups. The symbol ✓ is employed to indicate a lack of white layer (WL) or dark layer (DL) on the various tooth flanks and leads, thus implying that microstructural requirements were satisfied. By comparing the obtained data in terms of dimensional accuracy, surface roughness and microstructure, DRYs-3b was considered the optimal setup for the dry grinding process and was therefore chosen for subsequent steps introducing a double pass process for optimization and assessing the wear resistance of gears.

Table 10. Summary of microstructural analysis for dry hard grinding

	Left flank tip		*Left flank*		*Right flank tip*		*Right flank*		*Left lead*		*Right lead*	
	WL	*DL*	*WL*	*DL*	*WL*	*DL*	*WL*	*DL*	*WL*	*DL*	*WL*	*DL*
DRYs-1a	✘	✘	✓	✓	✘	✓	✓	✘	✘	✘	✓	✓
DRYs-1b	✘	✘	✘	✘	✘	✘	✘	✘	✓	✓	✘	✓
DRYs-2a	✘	✘	✘	✘	✘	✘	✘	✘	✘	✘	✓	✓
DRYs-2b	✘	✘	✘	✘	✘	✘	✘	✘	✓	✘	✓	✓
DRYs-3a	✓	✘	✓	✓	✓	✓	✓	✓	✓	✓	✘	✓
DRYs-3b	✓	✓	✓	✓	✓	✓	✓	✓	✓	✓	✓	✓

With the best setup chosen based on the previous SI results, a double pass configuration was developed based on the DRYs-3b configuration employing a fused aluminium oxide grinding wheel (GW-3) with a feed rate of 0.34 mm/rev and a total stock of 10 µm, which was divided into two passes with a stock of 5 µm. All dimensional parameters also fell within the specified tolerances in this case (blue bars in Figure 6).

In terms of surface roughness, comparable values of Ra were obtained to those achieved with the single pass process, with mean values of 0.36±0.015 µm and 0.22±0.025 obtained for the flank and lead, respectively. The resulting microstructure, shown in Figure 9, did not contain obvious defects, for which this setup was considered eligible for subsequent analyses.

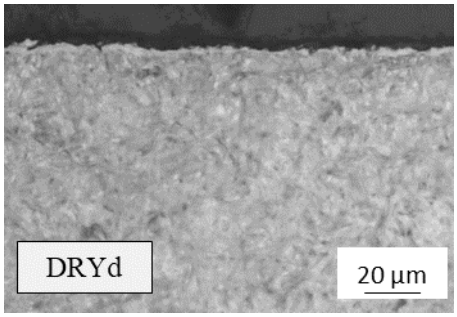

Figure 9 Microstructural analysis of sample obtained with dry hard double pass grinding

3.3 Superfinishing optimization

Analysis of gears subject to superfinishing led to the following outcomes:

- Dimensional analyses confirmed compliance of the process with the given requirements under all tested conditions. Detailed results are reported in Figure 10.
- Superfinishing achieved the lowest mean values of Ra, which were < 0.2 µm for all tested configurations. Roughness values are reported for both the tooth profile and lead in Table 11.
- The microstructure of gears finished with parameter groups SF-L1 and SF-L2, where the lowest depth of cut was employed for the second pass, did not contain obvious defects. SFH1 exhibited good results in terms of microstructure on the left flank but with a slightly darkened layer on the right flank (Figure 11a). SF-H2 (Figure 11b) instead exhibited both dark and white layers in all regions.

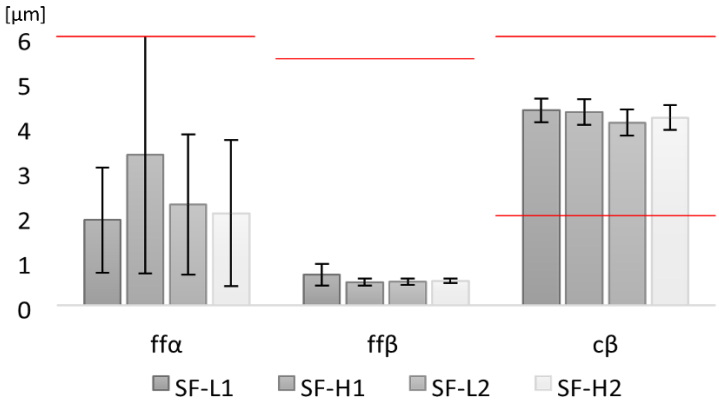

Figure 10 Dimensional tolerance measurements for superfinishing processes

Table 11. Measured roughness parameters for superfinished gears

	Profile Ra [µm]	*Std. Dev*	*Profile Rz [µm]*	*Std. Dev*	*Lead Ra [µm]*	*Std. Dev*	*Lead Rz [µm]*	*Std. Dev*
SF-L1	*0.15*	*0.01*	*1.05*	*0.14*	*0.06*	*0.01*	*0.45*	*0.08*
SF-H1	0.18	<0.01	1.22	0.08	0.09	0.01	0.54	0.06
SF-L2	0.16	0.01	1.12	0.14	0.07	0.01	0.44	0.06
SF-H2	0.17	0.01	1.16	0.15	0.09	0.02	0.51	0.09

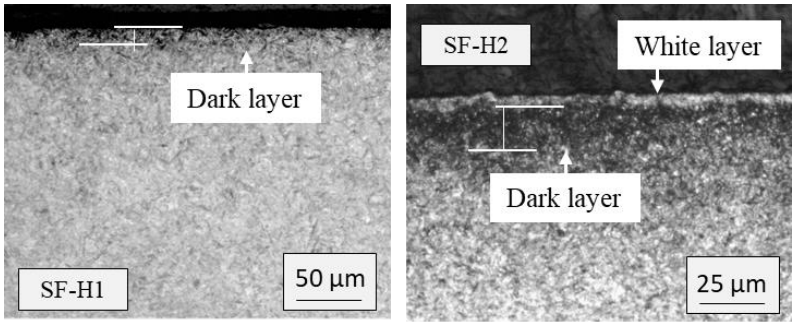

(a) (b)

Figure 11 Microstructural analysis of samples obtained with superfinishing performed with the highest stock on the second pass and D-GW-1 (a) and D-GW-2 (b) wheels

A summary of data obtained from microstructural analysis of gears subject to superfinishing is reported in Table 12. Configurations SF-L1 and SF_L2 achieved the best outcomes and were thus employed for subsequent analyses.

Table 12. Summary of microstructural analysis for superfinishing.

	Left flank tip		*Left flank*		*Right flank tip*		*Right flank*		*Left lead*		*Right lead*	
	WL	DL	WL	DL	WL	DL	WL	DL	WL	DL	WL	DL
SF-L1	✓	✓	✓	✓	✓	✓	✓	✓	✓	✓	✓	✓
SF-H1	×	×	×	×	✓	×	✓	×	✓	✓	✓	✓
SF-L2	✓	✓	✓	✓	✓	✓	✓	✓	✓	✓	✓	✓
SF-H2	✓	✓	✓	✓	✓	×	✓	×	✓	✓	✓	✓

3.4 Residual stress analysis

Table 13 presents the results of residual stress analyses performed on selected gears, achieving the best outcomes in terms of SI.

Table 13. Residual stress measurements in the middle of the flank of selected gears.

	σ0 [MPa]	σ90 [MPa]	τ0 [MPa]	τ 90 [MPa]
WET-1	-169	-555	-58	-106
DRYs-3b	192	-134	-78	-88
DRYd	94	-65	-88	-68
SF-L1	-405	-667	-55	-170
SF-L2	-304	-498	-49	-75

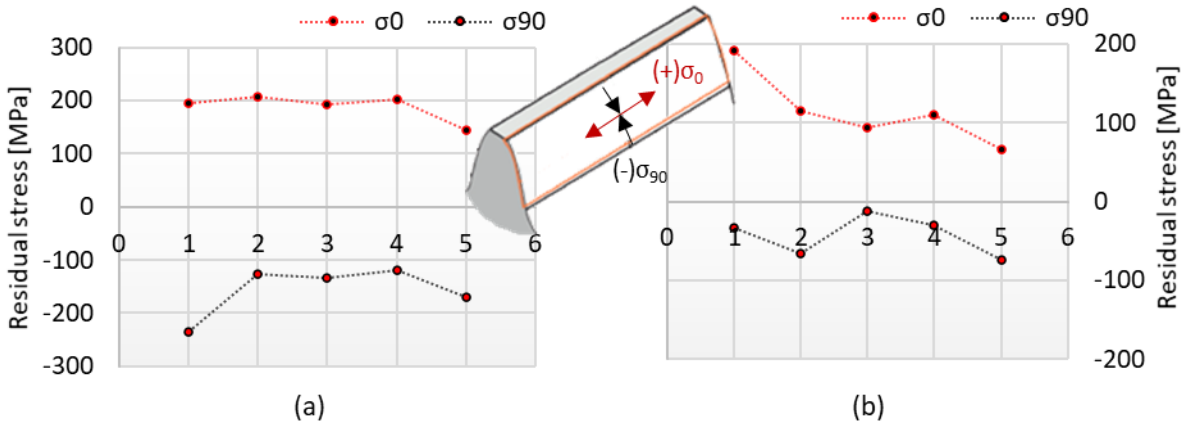

Figure 12 Residual stress maps in the flank profile (σ_0) and lead (σ_{90}) directions for dry hard grinding using setups DRYs-3b (a) and DRYd (b)

Positive values were measured on the flank profile with good repeatability between different probes (see Figures 12a and 12b, respectively, for DRYs-3 and DRYd), while stresses took on negative values in the lead direction. Both compressive and tensile residual stresses took on relatively low absolute values, suggesting that the thermal gradient had a relatively small impact overall. On the other hand, compressive stresses were observed in both directions following wet grinding and superfinishing, with the highest values occurring in the latter case.

3.5 Optical profiler analysis

Acquired surface topographies at the center of flanks finished with wet grinding, superfinishing and dry grinding with one and two passes are presented in Figure 13. Parallel valleys and crests were visible in the grinding lay direction, with smoother surfaces obtained with wet grinding and superfinishing and no major defects were observed under the tested grinding conditions. Average values of Sa, Ssk and Sku are presented in Table 14, together with standard deviation values. Trends in terms of average surface roughness were in line with linear values obtained from the Klingelnberg measuring system but with slightly higher values due to the consideration of a larger surface area. Wet ground and superfinished gears exhibited lowest Sa, followed by double-pass and then single-pass dry ground gears. Values of skewness (Ssk) were very close to 0, implying a symmetrical height distribution in all cases. This outcome implies a lack of critical features that could potentially accentuate gear noise, due to a prevalence of peaks for large positive values of Ssk, or wear and fatigue failure, due to a prevalence of valleys for large negative values of Ssk. Values of kurtosis (Sku) were greater than 3 for superfinished and wet ground gears, implying a leptokurtic distribution with sharp peaks. Dry ground gears also exhibited values of Sku greater than 3 but were much closer to a mesokurtic height distribution.

Table 14. Surface topography properties

	Sa [µm]	*Std. Dev*	*Ssk*	*Std. Dev*	*Sku*	*Std. Dev.*
WET-1	0.33	0.10	0.01	0.30	5.63	1.85
DRYs-3b	0.46	0.04	0.19	0.46	3.50	0.12
DRYd	0.44	0.06	-0.22	0.21	4.02	0.36
SF-L1	0.27	0.09	-0.12	0.36	6.00	1.77
SF-L2	0.32	0.09	0.35	0.18	8.13	3.85

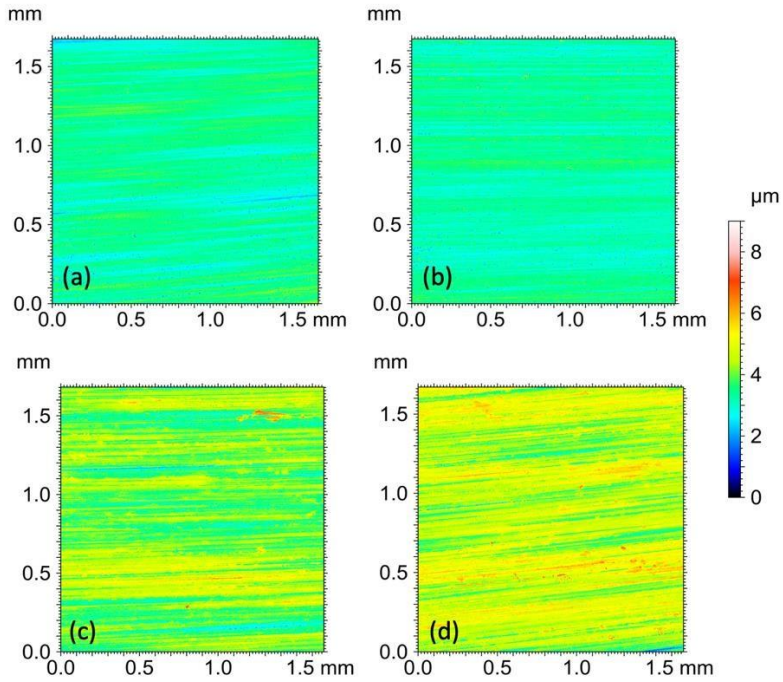

Figure 13 Acquired topography at the center of flanks ground with a) WET-1, (b) SF-L1 (c) DRYs-3b and (d) DRYd

3.6 Hardness results

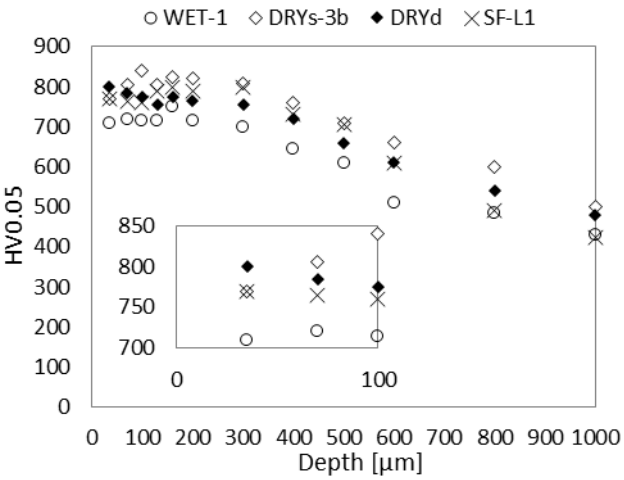

Figure 14 The measured hardness profile after wet grinding, superfinishing and dry grinding with one and two passes

The measured hardness profile after wet grinding, superfinishing and dry grinding with one and two passes are compared in Figure 14. The graph shows a comparable hardness profile trend of the gears after all machining processes but with a non-negligible difference in resulting values. The smaller box inside the graph highlights the measures in the first 100 µm below the flank surface and the following mean values can be calculated: 715 HV0.2 for WET-1, 805 HV0.2 for DRYs-3b, 787 HV0.2 for DRYd and finally 765 HV0.2 for SF-L1 condition. The mean values demonstrate a

hardness reduction due to the grinding process; however, in dry grinding conditions, the decrease is lower (about 25 %), while in wet conditions, this reduction is the maximum (about 33 %).

3.7 Wear test results

Images of gear, teeth acquired with a stereomicroscope after wear tests are shown in Figure 15. The contact pattern of the mating tooth can be seen on the faces of gear teeth with a light contrast. Dark grey regions were observed at the dedendum of some teeth, which were attributed to surface deformation resulting from severe contact conditions. Scuffing appeared as rough scratches on all teeth (white arrows in Figure 15), mainly in the upper part of the addendum but also at the dedendum of gear teeth ground under WET and SF-L1 conditions (Figure 15a and 15e). Micropitting only appeared at the dedendum of gear teeth ground under WET and SF-L2 conditions. The surface morphology was also examined using SEM to reveal microscopic features.

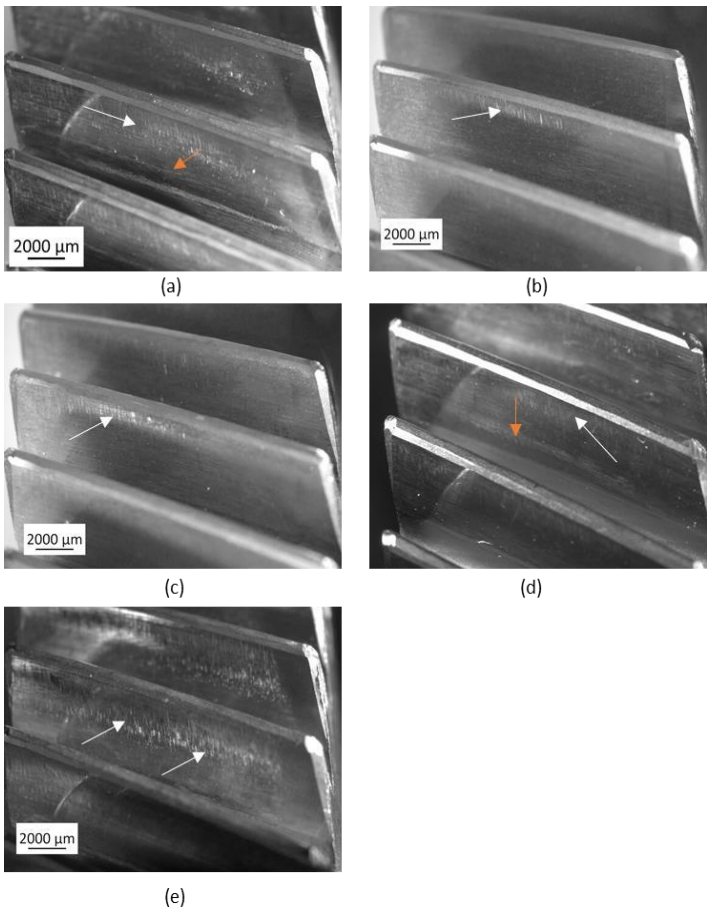

Figure 15 Images of gear teeth acquired with a stereomicroscope: WET-ground (a), DRYs (b), DRYd (c), SF-L2 (d) and SF-L1 (e). Scuffing and micropitting are highlighted with white and orange arrows, respectively

After grinding, the surface of each tooth was made up of parallel peaks and valleys with asymmetrical surface asperities running along the axial length. During wear testing, these asperities were plastically deformed in the direction of sliding and tended to cover nearby valleys (Figure 16). Micropits were left behind as these severely deformed asperities broke. Micropits formed in the opposite direction to sliding, in the same direction as the grinding lay.

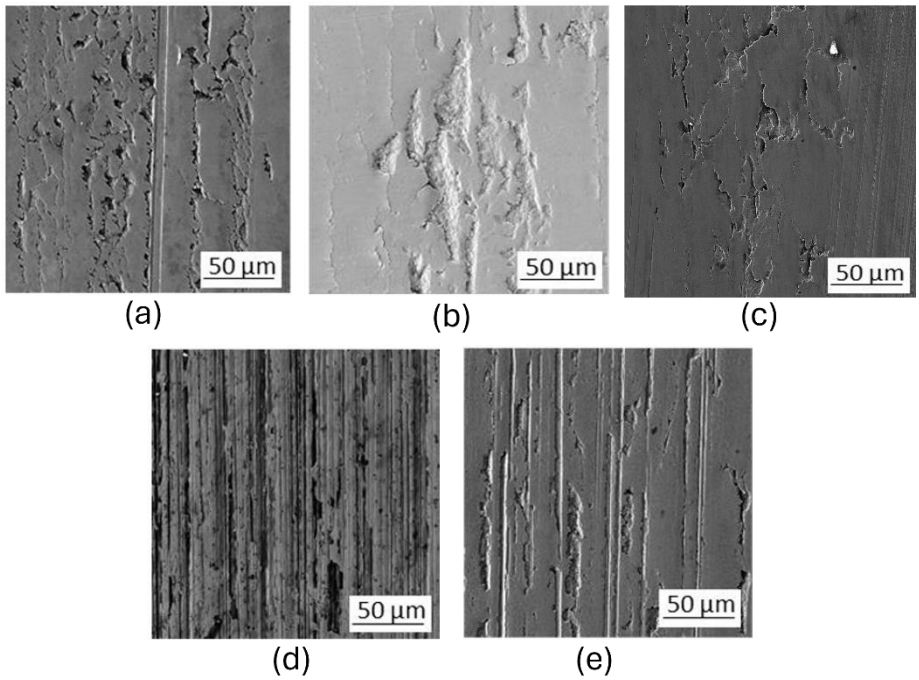

Figure 16 SEM images of tooth flanks subject to WET (a), Superfinishing D-GW-1 (b), Superfinishing D-GW-2 (c), DRYs (c), and DRYd (d) configurations after the wear test

The average wear area after 1.5 million cycles, calculated in line with Eqs. (1)-(3) in Section 2.4.1, is displayed in Figure 17 for all tested gears. Conventional wet ground gears exhibited an average wear area of 15.5% with a standard deviation of 2.8% across all tested samples. Dry grinding, both in single-pass (DRYs-3B) and double-pass (DRYd) configurations, improved wear resistance, with an average wear area of 11.4 % with a single pass and 9.1% with a double pass, with standard deviations of 1% and 0.6%, respectively. Results obtained with superfinishing were particularly interesting due to its perceived importance in improving industrial gear grinding processes. The average wear area following testing of gears prepared with the SF-L1 and SF-L2 setups was 18.4% and 17.4%, respectively, with standard deviations of 0.6% and 2.2%, implying worse wear resistance than all other finishing processes.

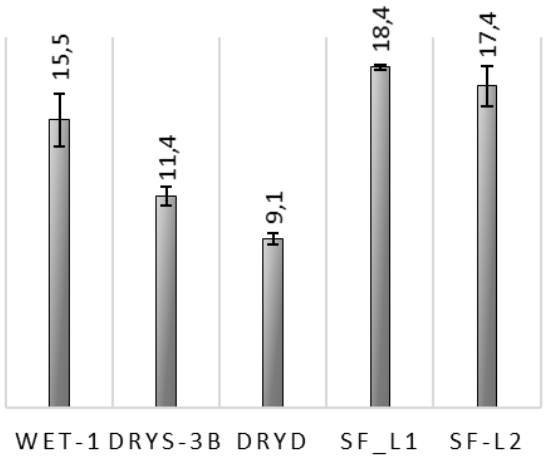

Figure 17. Average wear area ($A_{w,p}$) calculated for each grinding setup

4. DISCUSSION

The presented paper compared the effects, in terms of gear performance and surface integrity, of three different grinding processes: wet grinding, dry grinding and superfinishing. In the first part of the study, optimisation of cutting parameters was carried out for all selected processes, and the achievement of quality requirements in terms of geometric accuracy, roughness, microstructure and residual stresses was found in all conditions.

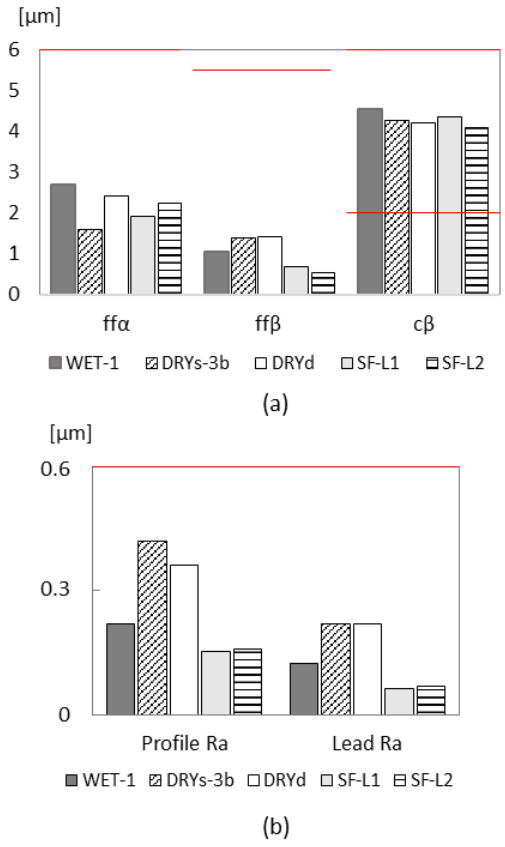

Figure 18: Dimensional tolerance (a) and roughness (b) comparison within optimised grinding conditions.

Klingelnberg measurements on dimensional tolerance show a substantial homogeneity between the processes, with no relevant differences between wet (conventional and superfinishing setups) and dry working conditions. Final values are much lower than commercial requirements in all cases (Figure 18a).

The flank and lead roughness measurements yield the same results when comparing the measured and required data, but after dry grinding, the roughness assumes higher mean values (Figure 18b), both after the single and double pass strategies. Despite this result, the in-depth analysis of surface topography carried out with the optical profilometers has shown that values of kurtosis (Sku) of dry ground gears were much closer to a mesokurtic height distribution. This outcome implies that superfinished and wet ground gears could potentially be more susceptible to wear and fatigue failure due to the lower radius of curvature of surface features compared to dry ground gears.

This result, together with the higher hardness measured in the subsurface of dry ground gears with respect to the wet ground, could be the explanation for the detected wear behaviour. The higher wear resistance shown by ground gears, in fact, would seem to be contradictory with the results of residual stress measurements [27-29]. The flank profile of gears subject to dry grinding shows slight tensile values as a result of a high thermal gradient, which also causes microstructural defects if grinding parameters are not optimized, as was previously discussed. Nonetheless, in the tested conditions of this study, high hardness and beneficial topography assume a higher weight with respect to residual stresses, and wear tests revealed that dry-ground gears have the longest durability.

Based on these results, dry grinding was proposed as an alternative to conventional wet grinding, able to satisfy the mechanical and geometric requirements of car manufacturers while improving wear resistance, reducing waste and increasing the sustainability of gear production in the strategic automotive market.

Summarizing the outcomes of this work, it was observed that (i) all finishing processes respected the given SI requirements; (ii) wet grinding and superfinishing achieved lower roughness, but dry ground Sku is much closer to a mesokurtic height distribution favouring the fatigue response in terms of wear; (iii) wet grinding and superfinishing resulted in compressive residual stress states while dry grinding resulted in tensile stress along the profile, but iv) the hardness of dry ground gears are higher in the sub-surface of the flank. In these described conditions, gears after dry grinding show lower flank wear compared to wet grinding and superfinishing.

5. CONCLUSION

In this paper, a comparison of FIAT 500 4/6 speed gears manufactured by FCA/Stellantis was performed, changing only the grinding process. The reference wet grinding process was compared with dry grinding and superfinishing processes. Three different grinding wheels were considered to account for the influence of the tool itself. The obtained results led to the following observations:

- There were no significant variations in the geometric accuracy of gears due to the grinding processes over the tested parameter range, with all three tested processes remaining within automotive manufacturer specifications.
- Wet grinding and superfinishing achieved lower roughness; but with sharper features detected with optical profilometer that could be detrimental for wear resistance.
- There were no significant variations in the microstructures of gears due to the grinding processes. Correct selection of process parameters allows ground surfaces to be obtained without burns or a white layer.
- Dry-ground gears show slight tensile residual stresses in the flank surface, but a higher hardness was measured below the same surface with respect to wet grinding conditions.
- The wear resistance of gears finished with dry grinding was considerably greater than that of gears finished with wet grinding or superfinishing. This is a fundamental advantage for electric vehicles, where noise must be minimized.

As a result, a different way of finishing gears for automotive applications based on a dry process was successfully implemented, providing important advantages compared to the current state of the art. Elimination of lubricant makes this solution more sustainable, improving wear resistance without compromising geometric accuracy.

Acknowledgement

Financial support from the European Commission for the European project FATECO (proposal number: 847284 Call: RFCS-2017) is gratefully acknowledged. Moreover, the authors would like to thank Ing. Michele Bandini and Ing. Marco Loberti and Peen Service for their technical support during residual stress measurements.

REFERENCE

[1] Gupta, K., Laubscher, R.F., Davim, J. Paulo, Jain, N.K., 2016. Recent developments in sustainable manufacturing of gears: a review. Journal of Cleaner Production 112, 3320-3330. https://doi.org/10.1016/j.jclepro.2015.09.133

[2] Gupta, K, Jain., Jain, N., Laubscher, R., 2017. Measurement of Gear Accuracy. Advanced Gear Manufacturing and Finishing. https://doi.org/10.1016/B978-0-12-804460-5.00007-9

[3] Karpuschewski, B., Knoche, H-J., Hipke, M., 2008. Gear finishing by abrasive processes. CIRP Annals Manufacturing Technology 57, 621-640. https://doi.org/10.1016/j.cirp.2008.09.002

[4] Karpuschewski, B., Beutner, M., Eckebrecht, J., Heinzel, J. and Hüsemann, T., 2020. Surface integrity aspects in gear manufacturing. Procedia CIRP 87, 3-12 https://doi.org/10.1016/j.procir.2020.05.112

[5] Li,H., Axinte, D., 2017. On a stochastically grain-discretised model for 2D/3D temperature mapping prediction in grinding. International Journal of Machine Tools and Manufacture 116, 60-76. https://doi.org/10.1016/j.ijmachtools.2017.01.004

[6] Brecher, C., Bäumler, S., Jasper, D., Triebs, J., 2012. Energy efficient cooling systems for machine tools. Proc. 19th CIRP Int. Conf. Life Cycle Eng. 239-244. http://doi:10.1007/978-3-64229069-5_41

[7] Teixeira, P.H.O., Rego, R.R., Pinto, F. W., de Oliveira Gomes, J., Löpenhaus, C., 2019. Application of hall effect for assessing grinding thermal damage. Journal of Materials Processing Technology 270: 356-364. https://doi.org/10.1016/j.jmatprotec.2019.02.019

[8] Shu, L. Fang, Z. Wang, C. Katsuma, T. Zhang, B. Sugita, N. 2023. Effect of single-grit wear on surface integrity of hardened stainless steel in dry grinding. CIRP Annals, Manufacturing Technology. https://doi.org/10.1016/j.cirp.2023.04.083

[9] Lerra, F., Liverani, E., Ascari, A., Fortunato, A., 2022. Prediction of the grinding wheel specification influence on thermal defects in dry grinding through a hierarchical FEM model. International Journal Advanced Manufacturing Technology. https://doi.org/10.1007/s00170-02209702-2

[10] Guerrini, G., Lerra, F., Fortunato, A., 2019. The effect of radial infeed on surface integrity in dry generating gear grinding for industrial production of automotive transmission gears. https://doi.org/10.1016/j.jmapro.2019.07.006

[11] Shu, L., Fang, Z., Wang, C., Katsuma, T., Zhang, B., Sugita, N., 2023. Prospects of dry continuous generating grinding based on specific energy requirement. CIRP Annals, Manufacturing Technology 72: 259-262. https://doi.org/10.1016/j.cirp.2023.04.083

[12] Budak, E., Jamshidi, H., 2021.On the prediction of surface burn and its thickness in grinding processes. CIRP Annals, Manufacturing Technology 70: 285-288. https://doi.org/10.1016/j.cirp.2021.04.041

[13] Karpuschewski, B., Knoche, H.J., Hipke, M., 2008. Gear finishing by abrasive processes. CIRP Annals Manufacturing Technology 57(2): 621 https://doi.org/10.1016/j.cirp.2008.09.002

[14] Mallipeddi, D., Norell, M., Sosa, M., Nyborg, L., 2019. The effect of manufacturing method and running-in load on the surface integrity of efficiency tested ground, honed and superfinished gears. Tribology International 131: 277–287. https://doi.org/10.1016/j.triboint.2018.10.051

[15] Zhou, W., Tang, J., Shao, W., 2020. Study on surface generation mechanism and roughness distribution in gear profile grinding. International Journal of Mechanical Sciences 187: 105921. https://doi.org/10.1016/j.ijmecsci.2020.105921

[16] Zhang, B., Liu, H., Zhu, C., Li, Z., 2019. Numerical simulation of competing mechanism between pitting and micro-pitting of a wind turbine gear considering surface roughness. Engineering Failure Analysis 104: 1-12. https://doi.org/10.1016/j.engfailanal.2019.05.016

[17] Wang, W., Liu, H., Zhu, C., Tang, J., Jiang, C., 2020. Evaluation of contact fatigue risk of a carburized gear considering gradients of mechanical properties. Friction 8: 1039-1050. https://doi.org/10.1007/s40544-019-0317-z

[18] Liu, H., Liu, H., Zhu, C., He, H., Wei, P., 2018. Evaluation of contact fatigue life of a wind turbine gear pair considering residual stress. Journal of Tribology 140: 041102. https://doi.org/10.1115/1.4039164

[19] Cui, L., Su, Y., 2022. Contact fatigue life prediction of rolling bearing considering machined surface integrity. Industrial Lubrication and Tribology 74 (1): 73-80. https://doi.org/10.1108/ILT08-2021-0345

[20] Hultgren, G., Mansour, R., Barsoum, Z., Olsson, N., 2021. Fatigue probability model for AWJcut steel including surface roughness and residual stress. Journal of Constructional Steel Research 179: 106537. https://doi.org/10.1016/j.jcsr.2021.106537

[21] Zhang, X., Wei, P., Parker, R., Liu, G., Liu, H., Wu, S., 2022. Study on the relation between surface integrity and contact fatigue of carburized gears. International Journal of Fatigue 165, 107203. https://doi.org/10.1016/j.ijfatigue.2022.107203

[22] Mallipeddi, D., Norell, M., Sosa, M., Nyborg, L., 2017. Influence of running-in on surface characteristics of efficiency tested ground gears. Tribology International 115: 45-58. https://doi.org/10.1016/j.triboint.2017.05.018

[23] Mallipeddi, D., Norell, Naidu, V., Zhang, X., Näslund, M., Nyborg, L., 2021. Micropitting and microstructural evolution during gear testing-from initial cycles to failure. Tribology International 156: 106820. https://doi.org/10.1016/j.triboint.2020.106820

[24] Bergstedt, E., Lin, J., Andreasson, M., Bergseth, E., Olofsson, U., 2021. Gear micropitting initiation of ground and superfinished gears: Wrought versus pressed and sintered steel. Tribology International 160: 107062. https://doi.org/10.1016/j.triboint.2021.107062

[25] Malkin, S., Guo, C. “Fluid Flow in Grinding.” Grinding Technology. Industrial Press, New York (2008): pp. 231-255

[26] Guerrini, G., Landi, E., Peiffer, K., Fortunato, A., 2018. Dry grinding of gears for sustainable automotive transmission production. Journal of Cleaner Production 176: 76-88. https://doi.org/10.1016/j.jclepro.2017.12.127

[27] Yang, S., Jin, X., Engin, S., Kountanya, R., El-Wardany, T., Lee, S. 2023. Effect of cutting fluids on surface residual stress in machining of waspaloy. Journal of Materials Processing Technology 322: 118170. https://doi.org/10.1016/j.jmatprotec.2023.118170

[28] Azarhoushang, B., Daneshi, A., Lee, D., 2017. Evaluation of thermal damages and residual stresses in dry grinding by structured wheels. Journal of Cleaner Production 142: 1922-1930. https://doi.org/10.1016/j.jclepro.2016.11.091

[29] Salonitis, K., Kolios, A., 2015. Experimental and numerical study of grind-hardening-induced residual stresses on AISI 1045 steel. International Journal Advanced Manufacturing Technology 79:1443–1452. https://doi.org/10.1007/s00170-015-6912-x